Molecular Biology Reports (2024) 51:838
https://doi.org/10.1007/s11033-024-09763-4

ORIGINAL ARTICLE

Employing novel biocompatible composite scaffolds with bioglass 58S and poly L-lactic acid for effective bone defect treatment

Erfan Motalebzadeh[1] · Saideh Hemati[2] · Mohanna Akbarin Mayvani[3] · Marzieh Ghollasi[4]

Received: 23 February 2024 / Accepted: 26 June 2024

Abstract

Background Bioglass materials have gained significant attention in the field of tissue engineering due to their osteoinductive and biocompatible properties that promote bone cell differentiation. In this study, a novel composite scaffold was developed using a sol-gel technique to combine bioglass (BG) 58 S with a poly L-lactic acid (PLLA).

Methods and results The physiochemical properties, morphology, and osteoinductive potential of the scaffolds were investigated by X-ray diffraction analysis, scanning electron microscopy, and Fourier-transform infrared spectroscopy. The results showed that the SiO_2-CaO-P_2O_5 system was successfully synthesized by the sol-gel method. The PLLA scaffolds containing BG was found to be osteoinductive and promoted mineralization, as demonstrated by calcium deposition assay, upregulation of alkaline phosphatase enzyme activity, and Alizarin red staining data.

Conclusions These in vitro studies suggest that composite scaffolds incorporating hBMSCs are a promising substitute material to be implemented in bone tissue engineering. The PLLA/BG scaffolds promote osteogenesis and support the differentiation of bone cells, such as osteoblasts, due to their osteoinductive properties.

Keywords Bone marrow mesenchymal stem cells · Bioglass 58S · Osteogenic differentiation

Introduction

Tissue engineering is an interdisciplinary field that emerged almost 30 years ago, mixing principles from life sciences and engineering to evolve new tissues using biologics on their own or with supported scaffolds [1, 2]. When faced with severe diseases or tissue/organ loss, conventional pharmaceutical treatments are often inadequate due to poor biocompatibility and insufficient functionality in artificial organs. Moreover, organ shortages and the possibility of immune rejection during transplantation further exacerbate the situation [3]. Tissue engineering offers an alternative approach for repairing damaged areas of the body and regenerating tissues and organs without the typical problems associated with traditional treatments. The principles of tissue engineering include scaffolds, cells, and growth-stimulating signals.

Researchers value mesenchymal stem cells (MSCs) as a versatile alternative for repairing damaged tissues in tissue engineering. MSCs possess the desirable traits of multi-potency capacity, ease of harvesting and cultivation, and effectiveness in decreasing immune response [4, 5]. MSCs have been utilized for over one thousand clinical trials to address a variety of diseases, such as musculoskeletal defects, auto-immune diseases, and myocardial infarcts [6, 7]. Within the population of MSCs, bone marrow stromal cells (BMSCs) present considerable proliferative capacity, an affinity for attaching to plastic to produce fibroblastic-like colonies, and a capability to differentiate within numerous mesodermal lineages, including cartilage, muscle, bone, fat, and neural progenitors [8]. While MSCs could be much like cultured in vitro two-dimensional monolayers through

✉ Marzieh Ghollasi
ghollasi@khu.ac.ir

1 Department of Biology, Basic Science Faculty, Science and Research Branch, Islamic Azad University, Tehran, Iran

2 Department of Cellular and Molecular Biology, Faculty of Biology, Science and Research Branch, Islamic Azad University, Tehran, Iran

3 Department of Cellular and Molecular Biology, Faculty of Advanced Science and Technology, Tehran Medical Sciences, Islamic Azad University, Tehran, Iran

4 Department of Cell and Molecular Biology, Faculty of Biological Sciences, Kharazmi University, Tehran, Iran

Published online: 23 July 2024

conventional tissue culture techniques, these methodologies no longer offer a comprehensive and appropriate microenvironment for clinical trials [9].

Scaffolds have a vital role in tissue engineering by serving as an artificial extracellular matrix (ECM), which creates a structure for cells to differentiate, proliferate, adhere, and migrate into new tissues [10]. These scaffolds should be porous enough for cell culture, have interconnectivity, be biodegradable, biocompatible, and possess appropriate mechanical properties that mimic the native ECM [11]. The biomaterials of engineered tissues can interact with cells *via* physical and biological components of scaffolds to boost cell attachment and influence cell morphology. Scaffolds can also deliver growth factors to improve tissue regeneration and provide mechanical stability for damaged tissues [12]. Matching the mechanical characteristics of the scaffold with those of the ECM and surrounding cells is imperative, as it can significantly impact the behavior of seeded cells, their adhesion, and cell shape [13]. Multiple investigations have been carried out on the production of bone scaffolds using diverse technologies that affect osteoinduction and osteoconduction, using materials that can be either synthetic or natural, biodegradable or non-biodegradable [14].

While natural scaffolds can be advantageous due to their abundance in various living organisms, many reports have highlighted their immunogenicity, pathogenic impurities, and inferior mechanical properties [15]. Synthetic polymers, like PLLA, are biodegradable and have low immunogenic reactions. Additionally, they can be mass-produced and possess controlled degradation, nano or microstructure, and strength with excellent flexibility [16]. However, poor cell-material interactions of PLLA and limited osteoconduction have restricted its effectiveness in bone tissue regeneration [17].

The biological properties of PLLA nanofibers were improved by coating them with inorganic, synthetic, and biocompatible biomaterial, which helped enhance osteoblast differentiation and overcome their disadvantages [18]. The appealing properties of bioglass materials have led to their widespread use as a coating material in bone regeneration for biomedical purposes [19]. Through the release of ions, these inorganic substances can facilitate tissue therapy, bone development, osseointegration, and antibacterial action [20]. Many research studies have indicated the capacity for regeneration of bioactive glass material as an ideal material for use in scaffold materials and help osteoinductivity and biocompatibility as well as enhancement of bone differentiation of particular types of stem cells to promote new bone tissue formation [21, 22].

The initial variety of bioactive glass to be produced was the 45S5 bioactive glass *via* the melt-processing approach, which ultimately culminated in the discovery of the sol-gel synthesis. The bioglass (BG) has been verified to depict enhanced antibacterial effectiveness, bioactivity, and biocompatibility in comparison with the 45S5 BG, owing to its greater porosity and surface area. This bioactive glass contains 59% SiO_2, 36% CaO, and 5% P_2O_5 (in mol%) [23, 24]. Despite their advantages, these materials still face specific limitations, particularly concerning their mechanical properties, low tensile strength, fatigue resistance, elastic modulus, and fast degradation rate [25]. Therefore, the composite scaffold containing BG may be an ideal alternative to overcome the limitations of both BG coating and polymer.

The choice of materials and the methods of production are equally significant. There are various techniques to make ceramic or BG-based scaffolds, each with limitations and advantages. The sol-gel approach is suitable for examining and managing biochemical reactions. This technique produces glasses with a large specific surface area and high porosity at a low temperature [26]. The bioglass materials created using this process exhibit exceptional bioactivity because of the residual hydroxyl ions, micropores, and high specific surface area [27]. Although some studies reported bioactive and degradable scaffolds of various BG and PLLA composite for bone tissue regeneration [28, 29], this study focuses on the novel application of bioglass 58S using the sol-gel method combined with PLLA, providing a unique approach to achieving optimal bioactive properties for bone defect treatment. Additionally, a sol-gel technique has shown fabulous promise for producing bioglass for commercial use.

We synthesized bioglass 58 S using the sol-gel procedure, followed by the PLLA/BG composite scaffold fabrication used as a framework for the osteogenic differentiation of hBMSCs. We expect that combining BG and PLLA may enhance the mechanical properties and increase the compatibility of cells with the bone scaffold. This improvement will be instrumental in making the bone scaffold beneficial for medical purposes.

Materials and methods

Preparation of glass powders

We utilized the sol-gel method to create BG 58 S powder [30]. Specifically, 21.5 ml of tetraethyl orthosilicate (TEOS Si $(OCH_2CH_3)4$ 99%, Merck), 13.9 ml of distilled water, and 2.88 ml of nitric acid (HNO_3 65%, Sigma-Aldrich) were mixed with ethanol at room temperature for one hour with continuous stirring. 15.72 ml calcium nitrate tetrahydrate $(Ca\ (NO_3)_2\ 4H_2O$ 98%, Sigma-Aldrich) and 1.13 ml triethyl phosphate $((CH_3CH_2O)_3$ P 99%, Merck) were then added the solution. Each part should be stirred well for 30 min

to complete dissolution. Furthermore, we stirred the blend for an hour to ensure the completion of the hydrolysis process. We dropped 2 M ammonia solution prepared from a stock 25% (4 ml, Sigma Aldrich, Germany) to the mixture to reach the gel point, followed by continuous stirring to form a homogeneous gel. Subsequently, the gel was dried for 24 h at 70 °C and then calcined at 700 °C to facilitate the transformation of the gel into glassy particles, referred to as bioactive glass 58 S.

Fabricating nanofibrous scaffolds using PLLA

The scaffold fabrication began by dissolving 0.43 g of PLLA (Sigma-Aldrich, U.S.A) in 6 ml of chloroform (Merck, Germany) with a concentration of 7% w/v. The blend was gently swirled on a magnetic stirrer at a speed of 100–250 rpm until everything dissolved completely. Once the solution became homogenous, we added 1 ml of dimethyl formaldehyde to the blend and stirred further. Finally, the mixture was loaded into a 10 ml plastic syringe fitted with a stainless steel needle with an outer diameter of eighteen gauges (equivalent to 1.270 mm). The scaffolds were fabricated with an electrospun solution. During the electrospinning process, we maintained a distance of 15 cm between the nozzle and the mobile collector, and the collector speed was set at 400 rpm while applying a voltage of 15 kV and feeding the solution at a rate of 0.4 ml per hour. To enhance hydrophilicity, cell adhesion, and surface modification of nanofibers, we utilized a low-frequency plasma generator operating at 40 kHz in a cylindrical quartz reactor (Diener Electronics, Germany) for plasma treatment. Subsequently, the nanofibers underwent exposure to pure oxygen gas plasma (Diener Electronics, Germany) at a pressure of 0.4 bars for four minutes to complete the process.

Fabrication of PLLA/BG nanocomposite

We dispersed BG in 2 mg/ml ethanol to fabricate the nanocomposite. To avoid nanoparticle agglomeration, we sonicated the solution using an ultrasonic device (UP400S, Hielscher, Germany) at a frequency of 50 MHz for 10 min. Subsequently, PLLA was immersed in the BG suspension in ethanol on a shaker to allow nanoparticles to infiltrate the fiber's pores. The samples were dried at 37 °C for 24 h.

Bioglass and scaffold characterization

SEM assessment

The structure of BG, PLLA, and PLLA/BG were analyzed employing SEM (Hitachi S-4500, Japan) to assess their morphology.

XRD analysis

We performed XRD analysis on the test specimen surfaces to observe the formation of apatite in the glass conducted using a Cu-Kα radiation emitter (λ = 1.5405 Å) operating at 40 kV (INEL-Equinox-3000 instrument, France) (a range of 2θ values from 20° to 50°).

FTIR spectroscopy evaluation

We employed FTIR spectroscopy (Nicolet Avatar 660 model, United States) to study the formation of the apatite phase on the surface of the samples. This technique allowed us to measure alterations in functional groups within 400–4000 cm^{-1}, with a precision of 8 cm^{-1}. After the disc's preparation, we measured the infrared spectra, which involved pressing a combination of finely powdered BG and KBr at a weight ratio of 1:100.

In vitro studies

Human BMSCs culture

We purchased the hBMSCs from the cell bank of the Stem Cells Research Center (Tehran, Iran). Human BMSCs were cultured in each well at a density of 10^4 cells on a flask with 10% FBS (Gibco, Germany), 1% antibiotic, and 90% DMEM and antimicotic kept within a humidified (37 °C, 5% CO_2) when cultures became 80% confluences, hBMSCs were detached by 0.5% trypsin EDTA solution (Gibco, Germany). Detached cells were cultured in another flask to reach 80 confluencies for further experiments.

Validation of cell viability

The human BMSCs were seeded in a 96-well plate at a density of 10^4 cells per well. The cells were incubated with a culture medium containing Pen/Strep and 10% FBS in DMEM (5% CO_2 at 37 °C for a day). The cytotoxicity of BG, PLLA, and PLLA/BG was measured using an MTT assay and AO/EB performed from day 1 to 3 according to our previous experiments [16, 27]. At days 1, 3, and 5 post-treatment, a 100 µl aliquot of MTT solution comprising 10 µl MTT (5 mg/ml stock solution) and 90 µl DMEM was added to the wells, followed by incubation in 5% CO_2 at 37 °C. Following the incubation, the MTT solution was aspirated, and the supernatants were solubilized using 100 µl of Dimethyl sulfoxide (DMSO) purchased from Merck, Germany. Subsequently, cell viability was assessed by determining the absorbance at a wavelength of 570 nm by a microplate reader (BioTek Instruments, USA).

AO/EB (100 µg/ml EB and100 µg/ml AO, Sigma) staining was qualitatively employed to assess the cell viability of hBMSCs. We added the dual fluorescent staining solution to each well, and PBS was used to wash for two minutes. Following incubation with staining for 20 min, fluorescence microscopy (Nikon, Japan) was used to capture images for each well.

Differentiation of osteogenic

The basal media was aspirated and replaced with an osteogenic medium consisting of DMEM supplemented with 50 mg/ml ascorbic acid 2-phosphate, 10% FBS, 10 nM dexamethasone, and 10mM P-glycerophosphate (Sigma Chemical Co.) to induce differentiation of hBMSCs towards osteogenic lineages (5% CO_2; 37 °C for fourteen days).

Staining of Alizarin red

We performed Alizarin red staining on days seven and fourteen after differentiation to assess the osteogenic differentiation. Following removing the medium, hBMSCs were washed with PBS for two minutes and fixed using 4% formaldehyde (Merck, Germany) for 20 min (4 °C). The cells were then washed with PBS to eliminate the formaldehyde and stained with a 1% blend of Alizarin red (Merck, Germany) at pH = 7.2 and room temperature (five minutes). Subsequently, the stained bone cells were rinsed several times with distilled water to eliminate any unbound dye and imaged using light microscopy (Carl Zeiss-Axiovert, Germany).

ALP activity and calcium content assays

We utilized an ALP kit assay (Parsazmun, Iran) on days seven and fourteen to measure the activity of ALP *via* osteogenic differentiation of hBMSCs. The plates were first washed with ice-cold PBS, following which 200 µl of radioimmune precipitation assay (RIPA) was employed to extract entire proteins from the cells. The supernatants were centrifuged (15,000 g; 4 °C; 15 min) before being incubated with an ALP assay kit upon the manufacturer's instructions. The amount of ALP in specimens was quantified at a wavelength of 405 nm with a microplate reader (BioTeklnstruments, USA).

We evaluated calcium deposition in whole specimens utilizing a calcium assay kit (Parsazmun, Tehran, Iran) following seven- and fourteen- days of osteogenic differentiation. Firstly, samples were rinsed slowly with PBS. Then, we performed calcium extraction to homogenize employing 0.6 mol/L hydrochloric acid (Merck), and the mixture was shaken (4 °C for 40 min). Next, we added a calcium reagent working solution to the samples. We evaluated the color intensity using light at a wavelength of 550 nm and measured the calcium content with a standard solution.

RT-PCR

The expression of fundamental osteogenic markers, including osteocalcin, collagen type I (Col I), ALP, and Runx-2, was analyzed using RT-PCR assay on days seven and fourteen after osteogenic induction. Total cellular RNA was isolated from cells and cDNA synthesis was accomplished using a Revert Aid first-strand cDNA synthesis kit (Fermentas, Burlingame, Canada). We employed the cDNA in forty cycles of PCR on a Rotor-gene Q real-time analyzer (Corbett, Australia). RT-PCR was conducted with Maxima TM SYBRGreen/ROX qPCR Master Mix (Fermentas) by melting curve analysis to validate PCR specificity. We assess specimens in duplicate and the average values used for quantification. Finnaly, we normalized target genes against HPRT and calibrated them to TCPS. Table 1 shows the primer sequences used.

Statistical analysis

Outcomes were represented as standard deviation (SD) and mean. The distinctions among groupings were defined by one-way analysis of variance (ANOVA) using the SPSS 17 statistical package, and $P < 0.05$ was considered statistically significant. We employed Excel (Microsoft Office) package 2010 for plots.

Table 1 The primer sequences utilized in the RT-PCR analysis

Genes	Primer sequence (F, *R*, 5′→3′)	Length of product (bp)
Runx-2	GCCTTCAAGGTGGTAGCCCCGTTACCCGCCATGACAGTA	76
HPRT	CCTGGCGTCGTGATTAGTGTCAGTCCTGTCCATAATTAGTCC	125
Col I	TGGAGCAAGAGGCGAGAGCACCAGCATCACCCTTAGC	121
Osteocalcin	GCAAAGGTGCAGCCTTTGTGGGCTCCCAGCCATTGATACAG	80
Osteonectin	TCTTCCCTGTACACTGGCAGTTCAGCTCGGTGTGGGAGAGGTA	73
ALP	GCACCTGCCTTACTAACTCAGACACCCATCCCATCTC	162

Results

SEM observation

Nano-structure PLLA was observed on the samples (Fig. 1a), and there was no willow fiber content. Figure 1b shows the nano-sized BG synthesized using the sol-gel technique. Because of their surface energy, large surface area-to-volume ratio, and nano-scale size, nanoparticles can enhance their interactions with the host tissue, leading to accelerated biocompatibility and solubility properties. Figure 1c and d illustrate the nano-fibers structure of the composite scaffold, which incorporates innovative bioactive glass nanoparticles at different magnifications. Figure 1e showed the cell attachment on fabricated scaffold. The images revealed that the bioactive glass particles have been effectively integrated with the fibers, forming a rough and porous structure that closely resembles the extracellular matrix (ECM). This unique structure enhanced the binding of nonspecific sites.

FTIR and XRD analyses

Figure 2 presents the FTIR of PLLA, BG, and PLLA/BG. In Fig. 2a, the observed bands in the 755–1749 cm^{-1} attributed to the presence of ester bonds between the oxygen and carbon atoms in a carbonyl group (C = O), and bands in the region 859–1984 cm^{-1} are duo to C-O stretching in carbonate groups. An absorbance band at 1044 cm^{-1} is associated with the C-CH_3 bond and peaks at regions 1127 cm^{-1} and 1182 cm^{-1} are assigned to CH_3 and COC + CH_3, respectively. Bands at 1359–1451 cm^{-1} revealed CH_2 asymmetric bending and the stretching mode of the CH group in CH_3 was at 2996 cm^{-1}. In Fig. 2b, a FTIR spectrum of BG exhibits peaks at 471 cm^{-1} and 803 cm^{-1} that relate to the stretching and bending vibration of Si-O bonds, respectively, and the broadband at 1094 cm^{-1} is associated with Si-O-Si asymmetrical stretching. The bands at 1649 cm^{-1} and 3436 cm^{-1} in BG are due to the O-H bond stretching. In Fig. 2c, all the bands linked to BG and PLLA appeared in the FTIR of the composite scaffold mentioned in their graphs. These results indicate proper interaction between BG and PLLA and demonstrate the formation of an appropriate composite. The O-H present in PLLA can form hydrogen bonds with the surface SiOH groups of the BG, facilitating a stable but weak interaction that helps in the initial adherence of BG to the PLLA fibers. This interaction can be observed in the FTIR spectra, where the broadening of the O-H peak in the composite suggests increased hydrogen bonding.

Figure 3a shows the XRD spectrum of bioactive glass nanoparticles, and BG exhibited an amorphous glass phase. The XRD spectrum of PLLA/BG is shown in Fig. 3b. The structure exhibited a completely amorphous and non-crystalline phase, with overlapping peaks corresponding to BG and PLLA. Notably, the peaks around 10 exhibited higher intensity, particularly in the range of 31, which can be attributed to the presence of both BG and PLLA.

These XRD results are consistent with the FTIR findings confirming the PLLA/BG scaffold formation.

In vitro biocompatibility

Figure 4 illustrates how BGs and PLLA affect the viability of the hBMSCs cell line by MTT assay. One day after treatment began, BG demonstrated a statistically significant difference compared to the control ($*P < 0.05$). We observed no significant difference in the formazan formation among the control, PLLA, and PLLA/BG groups ($*P > 0.05$). On 3rd day of treatment, BGs significantly increased in the growth of hBMSCs. Although the PLLA and PLLA/BG groups gave rise to hBMSCs proliferation, there are no statistically significant differences compared to a control group. Over five days, hBMSCs exhibited remarkable growth in the vicinity of PLLA/BG and BG groups, which showed the BGs' effectiveness on PLA composition on the hBMSCs proliferation.

To study the hBMSCs viability in the existence of PLLA, BG, and PLLA/BG groups, we cultured cells for five days and then stained them with AO/EB (Fig. 5). The hBMSCs proliferation on the BG, PLLA, and PLLA/BG groups just recognized as usual in comparison with the control group. The groups did not have a cytotoxic effect on hBMSCs growth and did not decrease the cell viability and proliferation of the hBMSCs.

Therefore, no cytotoxic effect of groups was observed for hBMSC's growth, and none of them enhanced the apoptosis rate in the hBMSC's, as demonstrated by both MTT assay and AO/EB staining. The combination of these two methods provided a comprehensive assessment of cell viability and

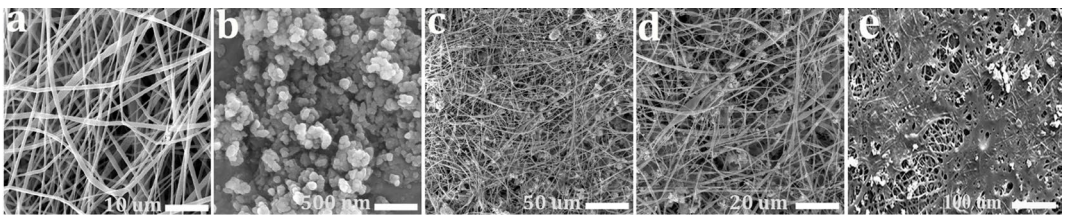

Fig. 1 SEM Images, **(a)** PLLA nanofibers, **(b)** BG, (**c** and **d**) PLLA/BG nanocomposite, and **(e)** PLLA/BG nanocomposite with cells

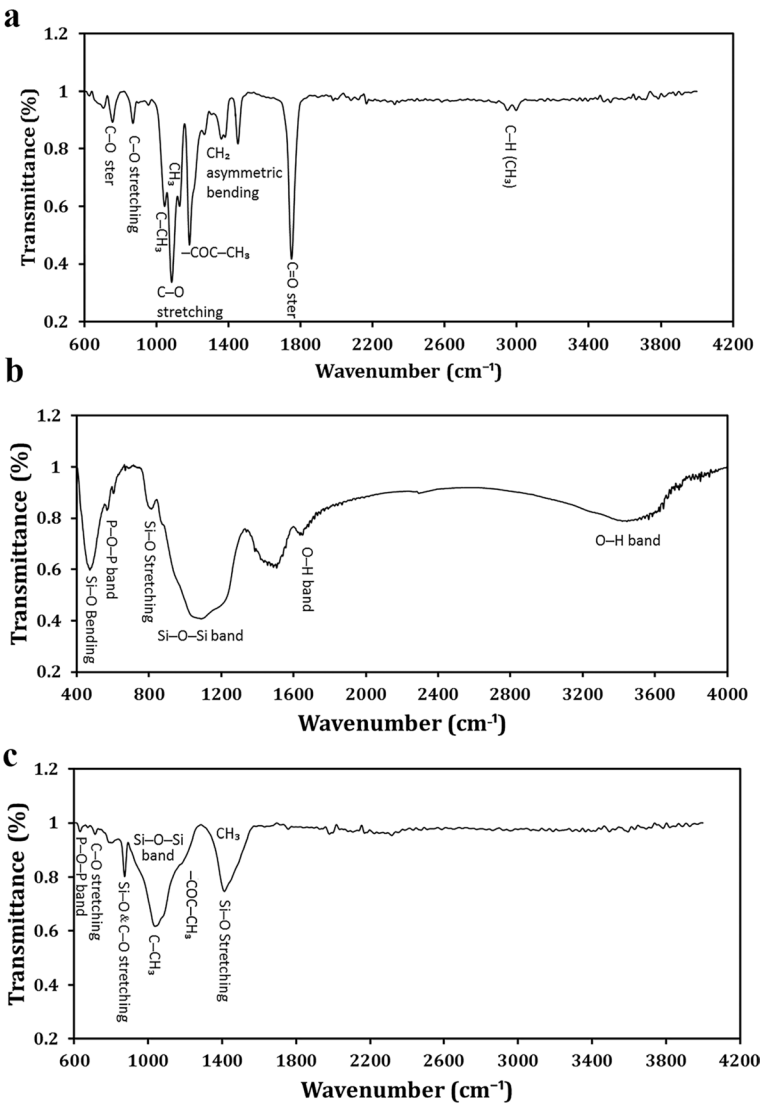

Fig. 2 Spectra of FTIR of **(a)** PLLA, **(b)** BG, and **(c)** PLLA/BG nanocomposites

apoptosis, confirming that the scaffolds are biocompatible and safe for further application.

ALP activity and mineralization measurement

We evaluated the activity of ALP in hBMSCs in the existence of BG, PLLA, and PLLA/BG after seven and fourteen-day osteogenic induction. On the 7th day, the hBMSCs treated with BG and PLLA/BG were observed to have higher ALP activity than in the control group (Fig. 6a). In addition, remarkably more ALP activity was seen in BG and PLLA/BG groups following a fourteen-day induction (Fig. 6a), which means that the BG and PLLA/BG enhanced the up-regulation of ALP the expression.

Calcium biomineralization occurs when osteoblast cells secrete minerals into the ECM in the final stage of osteogenic differentiation, serving as a marker of the successful completion of this process. Figure 6b displays the outcomes acquired from quantifying calcium deposition, demonstrating that the PLLA/BG and BG groups had a higher calcium content than the control group on day seven. Moreover, the mineralization of hBMSCs treated with BG and PLLA/BG was more than nanocomposite lacking bioactive glass, as indicated by a statistically significant ($P < 0.05$).

Alizarin red staining

Figure 7 illustrates the measurement of hBMSCs mineralization *via* Alizarin red staining. Hence, the Alizarin red stain combines with calcium to form a chelate, an orange-red color is produced, and cells induced with osteogenesis exhibit nodule formation. It can be observed from Fig. 7 that hBMSCs treated with BG, PLLA, and PLLA/BG displayed varying degrees of matrix mineralization. In particular, cells treated with BG had higher calcium nodules following fourteen days of incubation vs. the group of control (Fig. 7b).

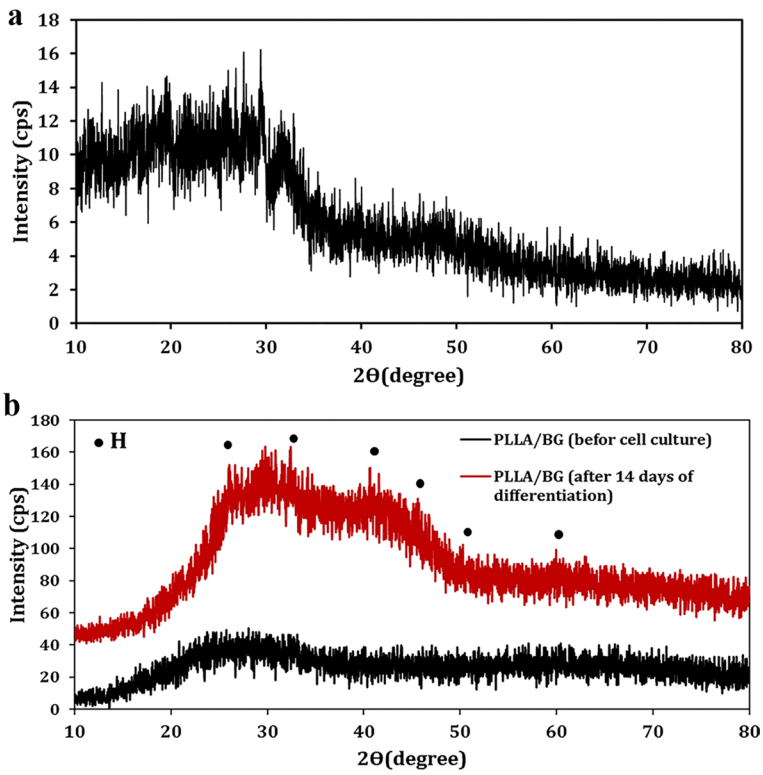

Fig. 3 XRD patterns of **(a)** BG and **(b)** PLLA/BG nanocomposites

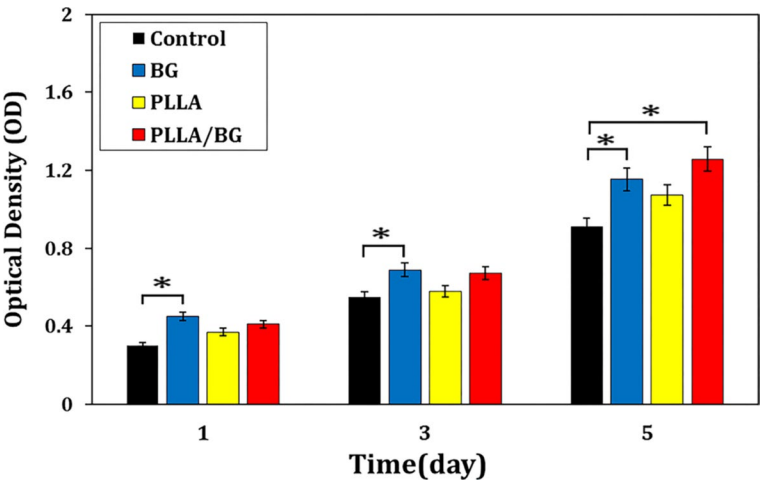

Fig. 4 The hBMSCs optical density after 1, 3, and 5 days in the presence of control, BG, PLLA, PLLA/BG (*$p < 0.05$)

Figure 7c demonstrates that the hBMSCs treated with the PLLA scaffold experienced a minimal increase in nodule formation compared to the control and BG-treated hBMSCs. However, PLLA in the presence of BG led to nodule formation in treated cells (Fig. 7d). Based on the findings, a combination of BG and PLLA scaffold could boost the formation of bone-like nodules in hBMSCs following fourteen-day osteo-induction.

RT-PCR

Figure 8 indicates the comparative expression of bone-related genes such as Col I, osteocalcin, osteonectin, RUNX-2, and ALP. Across the board, the relative expression levels of osteocalcin, ALP, Col I, and osteonesctin displayed an upward trend, increasing from day seven to fourteen. The nano-composite scaffolds exhibited the highest expression levels of these genes. On day seven (Fig. 8a), the ALP expression remarkably increased in hBMSCs treated with BG and PLLA/BG compared to those of the control ($P < 0.05$). Although the expression level of the ALP gene in the PLLA group was higher than the control, Data did not show any statistically significant difference vs. the group of control. Fascinatingly, osteocalcin gene expression became upregulated in hBMSCs of BG and PLLA/BG groups more than those of the control. BG and PLLA/BG

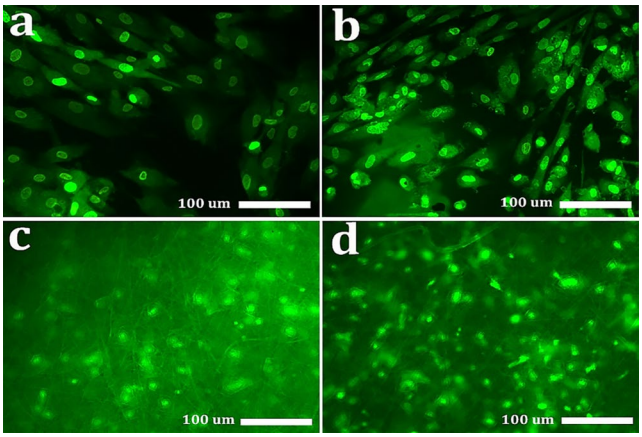

Fig. 5 The nuclear staining by acridine orange of hBMSCs cultured on **(a)** control, **(b)** BG, **(c)** PLLA, and **(d)** PLLA/BG on day five under a fluorescence microscope

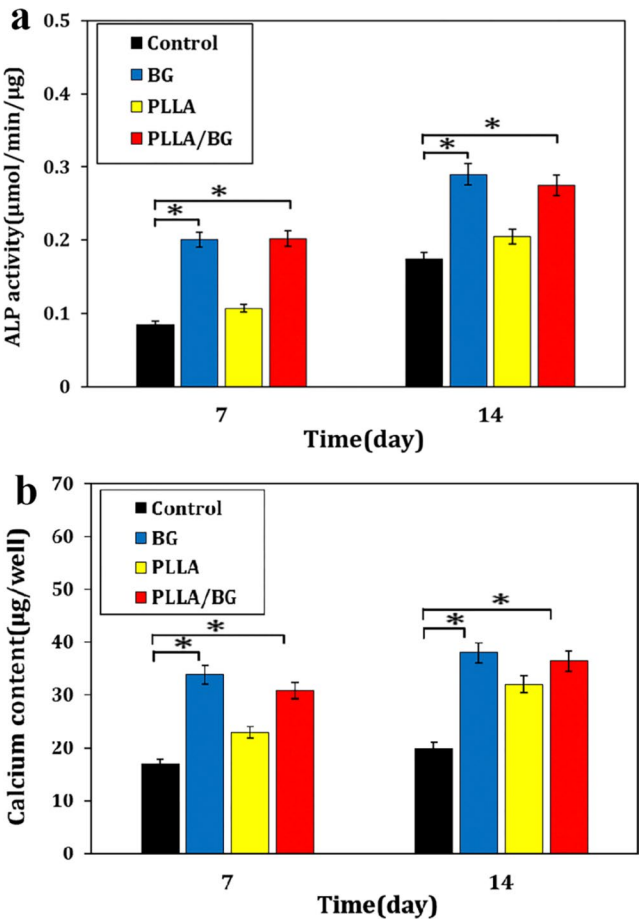

Fig. 6 **(a)** ALP activity and **(b)** calcium deposition of hBMSCs in the presence of control, BG, PLLA, and PLLA/BG after seven and fourteen days under differentiation medium (*$p < 0.05$)

groups increased Col I gene expression more than the control ($P < 0.05$). The osteonectin gene expression level was significantly increased in hBMSCs near the PLLA/BG and BG groups compared to the control ($P < 0.05$). Although the RUNX-2 gene expression rose in entire groups *versus* control (Fig. 8a). On day fourteen, high differences were observed in ALP, osteocalcin, osteonectin, and Col I of hBMSCs treated with BG and PLLA/BG groups vs. control (Fig. 8b). On the other hand, the RUNX-2 gene expression level in all groups decreased compared to those on day seven.

Discussion

Since bone defects lead to dramatic costs worldwide, a growing concentration has focused on developing artificial biomaterials for tissue (bone) regeneration. The regeneration capacity of composite materials depends on interactions between cells and material [32]. Numerous studies revealed that some bioactive components positively impact regulating cellular function, such as attachment, migration, proliferation, and differentiation [33]. According to in vivo studies, bioglass-based compositions produce no cytotoxicity and inflammation [34]. Yang et al. demonstrated that composite scaffolds containing bioactive glass served hBMSCs adhesion, growth, and osteogenesis in vivo and in vitro [35]. According to different research, the biocompatibility of stainless steel and its ability to bond with bones can be improved by implementing a coating of bioactive glass on the substrate by the sol-gel technique [36]. Hence, this study employed biocompatible composite scaffolds incorporating bioactive glass to create a degradable porous three-dimensional structure that can support cell proliferation and growth while promoting differentiation into bone lineages for effective bone defect treatment.

In the current study, with the sol-gel method, the SiO_2-CaO-P_2O_5 system was successfully synthesized (according to SEM, XRD, and FTIR data). A sol-gel technique used in the production of bioactive glass offers a favorable substitute for the process of traditional melt-quenching. This technique is carried out at ambient temperatures, improving the purity and homogeneity of the glass, consequently resulting in a broader scope of compositional possibilities [37]. Moghanian et al. successfully synthesized bioactive glass containing various amounts of Li_2O with the technique of sol-gel [38]. Sol-gel-derived glasses represent a higher rate of hydroxyapatite formation vs. the melt-quenching method. Also, it is relatively more straightforward to achieve biodegradability and bioactivity in such glasses [39, 40]. The XRD chart demonstrated that the bioactive glass in its initial form possessed an amorphous structure, confirming the sol-gel method can create glasses of exceptional purity [36]. The absence of diffraction peaks for BG, and instead a broad band from 15 to 35° in 2θ, corresponds well with an amorphous BG structure [38, 41]. The FTIR analysis of the

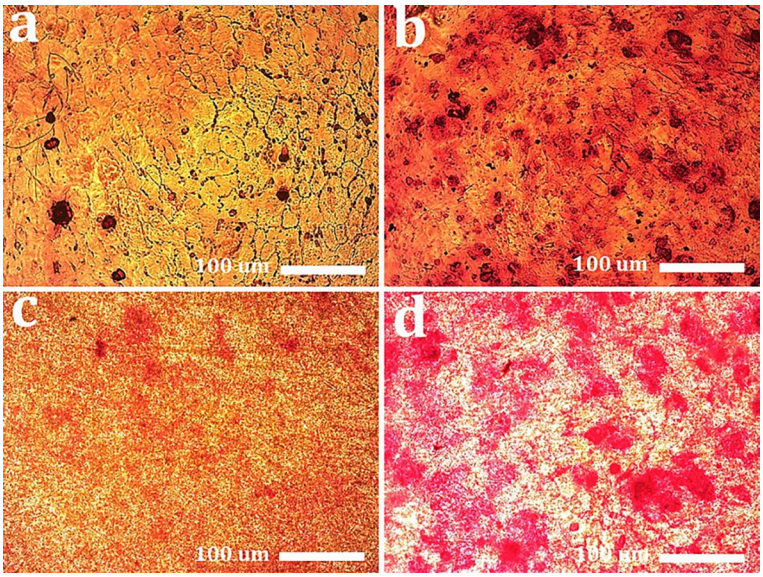

Fig. 7 Alizarin red staining of hBMSCs under the light microscope **(a)** control, **(b)** BG, **(c)** PLLA, and **(d)** PLLA/BG on day fourteen differentiation

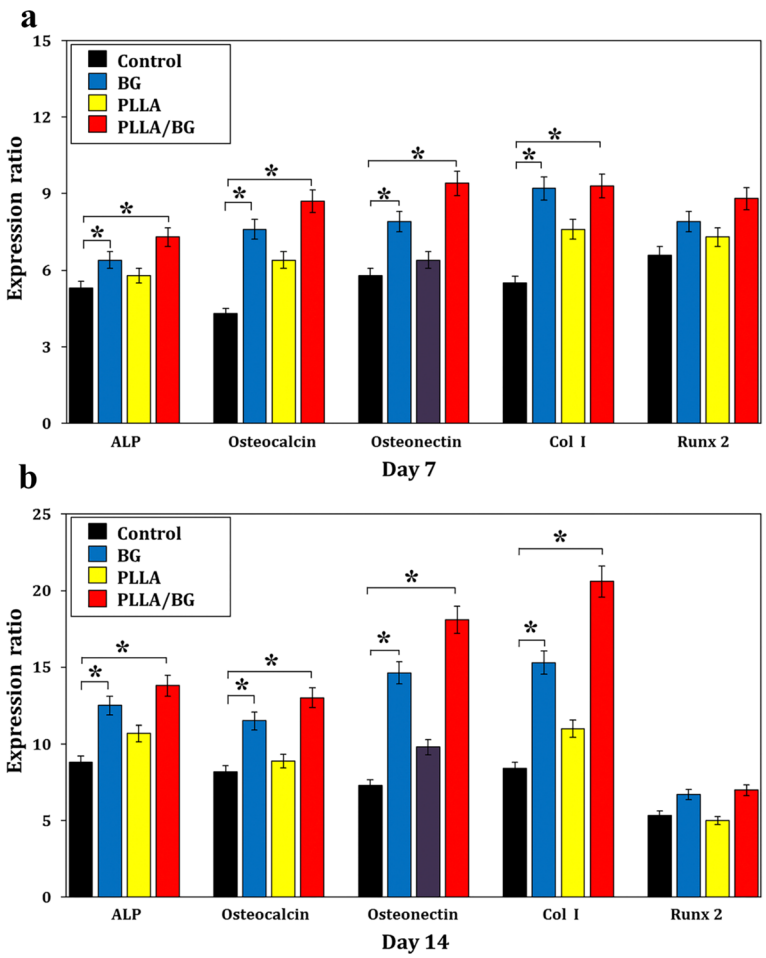

Fig. 8 The osteogenic markers expression level in hBMSCs in the existence of control, BG, PLLA, PLLA/BG after **(a)** seven and **(b)** fourteen days in the differentiation medium (*$p < 0.05$)

synthesized BG revealed characteristic bands in the spectra. Specifically, the bands observed at 471 cm^{-1} were assigned to the bending mode of Si-O bonds, while the broadband observed at 1094 cm^{-1} was attributed to the asymmetrical stretching of Si-O-Si bonds [42, 43]. In BG, the band observed at 1649 cm^{-1} is attributed to absorbed water and the O-H bonds stretching from silanol groups (Si-OH) [41]. A peak observed at around 3436 cm^{-1} is linked with the existence of -OH groups [32]. Cell attachment could refer to SiO_2 and P_2O_5 in bioactive glasses for network-making

factors. In addition, Si-OH, generated with an exchange of Ca^{2+} with H_3O^+, could boost hBMSCs' adhesion and growth. Moreover, it has been reported that Si^{4+} and Ca^{2+} discharging from BG into the cell culture medium is crucial for promoting cell differentiation and proliferation, leading to gene overexpression [44]. These ions can interact with the COOH and -OH groups in PLLA, further stabilizing the composite structure and promoting bioactivity. The interactions between BG and PLLA can be attributed to Van der Waals forces and hydrogen bonds. The incorporation of BG enhances these interactions by providing additional sites for protein adsorption, thus supporting cellular activities. These interactions collectively contribute to the formation of a composite scaffold with improved bioactivity and suitability for bone tissue engineering.

Microstructure and surface attributes of a scaffold, including fiber size, pore distribution, surface roughness, overall porosity, and coated material shape, can significantly influence its biological properties [45]. PLLA is known as biocompatible and biodegradable implants, which provide a proper condition as ECM for the growth of various MSCs and generated bone-like tissue [16]. Noticeable surface roughness in PLLA scaffolds synthesized through the electrospinning process observed in our study. Electrospun nanofibrous matrices possess similar structures to the ECM, along with high porosity, extended surface area-to-volume ratio, and varying distribution of pore size, which could influence cellular behavior [46]. After the addition of BG, no tangible changes in the morphology of the nanofibers were seen in the microstructure. Bioactive materials need to be able to bind with the bone tissue by forming hydroxyapatite on their surface. The bioactivity of BGs is associated with their capacity to develop a hydroxyapatite layer on their surface, which leads them to a structure and composition similar to natural bone [47]. Previous studies have indicated that polymers supplemented with BG exhibit full surface coverage with apatite residues. This phenomenon contributes to their enhanced biocompatibility, differentiation, cell growth, and mechanical properties [48]. Radev's study demonstrated the formation of nanohydroxyapatite on the surface of a PU/85S after incubation in SBF. This composite material is beneficial in bone tissue engineering applications [49]. Additionally, bioactive glasses are particularly useful in counteracting the acidic environment that arises from the degradation of biopolymers, which is harmful to cells [48].

For the second part, the biocompatibility of BG, PLLA, and PLLA/BG was investigated in combination with hBMSCs. This step will provide valuable insights into the safety and suitability of the scaffolds for further research and application. A key aspect of this evaluation was to ensure that these scaffolds do not exhibit cytotoxic effects. The MTT assay, widely used to measure cell viability by assessing mitochondrial activity, was complemented with AO/EB staining. This staining allows for the visualization of live and dead cells, diferentiating between viable, apoptotic, and necrotic cells, thus providing a more comprehensive assessment of cell viability and apoptosis. Both the MTT assay and AO/EB staining consistently indicated that there were no cytotoxic effects of the BG, PLLA, and PLLA/BG scaffolds on hBMSCs' proliferation. The AO/EB staining confirmed the findings of the MTT assay by showing a high proportion of live cells and a negligible presence of dead cells across all scaffold groups. Shahrbabak et al. showed that BG had no cytotoxic impact on G292 osteoblastic proliferation after seven days of experiment [50]. Barrioni et al. discovered that the mitochondrial activity of hMSCs notably increased after a four-day exposure to the dissolution products of BG vs. the control [51]. The comprehensive assessment using both MTT and AO/EB staining demonstrated that BG, PLLA, and PLLA/BG scaffolds are biocompatible and do not exhibit cytotoxic or pro-apoptotic effects on hBMSCs. Cell growth was accelerated on the 5th day, specifically for the PLLA/BG group ($^{**}P < 0.01$), suggesting that the combination of PLLA/BG has a more significant impact on the proliferation of hBMSCs compared to BG or PLLA alone. We observed for the first time that coating the PLLA scaffold with BG makes a favorable surrounding for proliferation and osteoblastic differentiation in our research. Significantly, the cells remained viable for two weeks, even though the proliferative activity indicated that cells on the PLLA/BG samples exhibited superior growth compared to the other samples. This combined approach provides robust validation of the scaffolds' safety and suitability for further research and potential biomedical application.

The findings from the staining of Alizarin red indicated that hBMSCs cultured under osteogenic circumstances (in vitro) witnessed a shift in cell morphology, which produced ECM with calcium-rich deposits (more bone-like cells). Prior research has documented the ability of BGs to accelerate the proliferation, differentiation, and adherence of osteogenesis-related cells [52]. The data presented indicates that hBMSCs treated with BG formed osteo-like cells and showed positive Alizarin red, suggesting the presence of calcium-rich depositions. Moreover, these findings showed that BG, along with the PLLA scaffold, is osteoinductive and promotes mineralization, as confirmed by the deposition of calcium assay and upregulation of ALP enzyme activity. Yao et al. found that rabbit MSCs showed increased ALP activity when cultured on GF/BG scaffolds compared to scaffolds without BG from day seven to day fourteen [53]. When ovarian follicular fluid MSCs were cultured on bioglass with osteogenic factors, they showed increased cell viability, ALP activity, calcium deposition,

and bone-specific protein production compared to those uncoated titanium [22].

These results were more supported by the RT-PCR findings, where BG-based scaffold significantly gave rise to Col I, ALP, osteocalcin, and osteonectin characteristic of more mature bone cells. ALP, RUNX-2, and osteocalcin were upregulated in the monolayer (human dental pulp stromal cells) cultured on 45S5 bioglass and in osteogenic conditions at fourteen days vs. groups of control in the basal medium [54]. The ALP gene is a premature indicator of the maturation process of the osteoblasts. It is initially detected in bone-like cells that tend to differentiate into osteoblasts [55]. Col I is expressed during the later stages of cell proliferation and has a function in both the mineralization and differentiation of osteoblasts [56]. Research showed that gene expression such as Col I, ALP, and Runx-2 stood higher for the MSCs treated with the scaffold containing BG than those treated with the scaffold without BG [53]. There was no significant variation in RUNX-2 expression among PLLA/BG and other groups and the control group on day seven. Still its expression level was higher in hBMSCs cultured in BG and PLLA/BG groups. Despite observing a similar trend on day fourteen, RUNX-2 expression decreased in cells cultured on all groups, especially PLLA scaffolds, during the second week. RUNX-2 acts in the initial orientation of MSC differentiation towards osteogenic lineages. Its expression represents the highest in the early stages of differentiation and subsequently decreases [57]. Under all culture conditions, osteocalcin and osteonectin gene expression boosted compared to control on days seven and fourteen, indicating hBMSCs differentiated into bone-like lineages. Osteonectin is a glycoprotein and is considered a binding factor of collagen chains or ions of calcium. It is crucial for the initiating biomineralization and the nucleation of hydroxyapatite crystals [58, 59]. Osteocalcin consists of three carboxyglutamic acids and is known as the most significant gene involved in osteogenic differentiation. It is expressed late in the osteogenic process of differentiation and contributes to the formation of bone by affecting the absorption of calcium [60]. These findings imply that the PLLA and BG scaffold's synergistic impact leads to osteogenic differentiation of hBMSCs.

Multiple studies have provided evidence supporting the wingless (Wnt) involvement signaling pathway in the differentiation of stem cells into osteoblasts [61]. In this pathway, β-catenin plays a crucial role as a signaling factor [62]. Additionally, the Akt signaling pathway activation has been linked to the inhibition of glycogen synthase kinase-3 (GSK3β), leading to the translocation and accumulation of β-catenin, which has a significant role in the regeneration of bone [32]. Zhu et al. observed a rapid increase in the Akt/GSK3β signaling pathway upon treatment with a BG-containing scaffold, and inhibition of this pathway resulted in the suppression of ALP activity [28]. These outcomes indicate that BG in the scaffold activates the Akt/GSK3β signaling pathway, thereby inducing hBMSCs osteogenic differentiation.

Conclusion

In the current survey, the SiO_2-CaO-P_2O_5 bio-active glasses were successfully synthesized by the sol-gel method according to SEM, XRD, and FTIR. Moreover, considerable surface roughness was observed in the PLLA scaffolds synthesized by electrospun. Human BMSCs continued to increase after five days of cultivation on 58S5 bioglass combined with PLLA, as confirmed by MTT assay and AO/EB staining. The findings confirmed that BG, along with the PLLA scaffold, is osteoinductive and promotes mineralization, as demonstrated by the calcium deposition assay, upregulation of ALP enzyme activity, and the Alizarin red staining data. These results were more supported by the real-time PCR findings, where bioglass-based scaffold gave rise to ALP, osteocalcin, osteonectin, Col I, and RUNX-2, characteristic of more mature osteoblasts. The in vitro study showed that scaffolds based on 58S5 bioglass combined with PLLA are promising structures for osteogenic differentiation of hBMSCs. These composite scaffolds with hBMSCs provide magnificent alternative materials for bone tissue engineering applications. However, prior to in vivo study, more assessments such as mechanical properties of scaffolds are essential.

Acknowledgements The support of the Research Council of Kharazmi University is highly appreciated. We thank Ms. Elahe Eftekhari for her assistance with this project.

Author contributions EM: Investigation, Data curation, Original draft preparation. SH: Methodology, Visualization, Formal Analysis, and Writing. MAM: Methodology, Visualization, Formal Analysis, and Writing. MG: Administration, Conceptualization, Supervision, Validation, Writing – Review & Editing.

Funding The authors declare that no funds, grants, or other support were received during the preparation of this manuscript.

Data availability No datasets were generated or analysed during the current study.

Declarations

Ethics approval and informed consent Not applicable. This article does not contain any studies with human participants or animals performed by any of the authors.

Competing interests The authors declare no competing interests.

References

1. Langer R, Vacanti J (2016) Advances in tissue engineering. J Pediatr Surg 51:8–12
2. Vacanti CA (2006) The history of tissue engineering. Journal of cellular and molecular medicine
3. Ikada Y (2006) Challenges in tissue engineering. J Royal Soc Interface 3:589–601
4. Jin Q, Yuan K, Lin W, Niu C, Ma R, Huang Z (2019) Comparative characterization of mesenchymal stem cells from human dental pulp and adipose tissue for bone regeneration potential. Artificial Cells, Nanomedicine, and Biotechnology 47, 1577–1584
5. Masoumi N, Ghollasi M, Raheleh H, Eftekhari E, Ghiasi M (2023) Carbachol, along with calcium, indicates new strategy in neural differentiation of human adipose tissue-derived mesenchymal stem cells in vitro. Regenerative Therapy 23:60–66
6. Gomez-Salazar M, Gonzalez-Galofre ZN, Casamitjana J, Crisan M, James AW, Péault B (2020) Five decades later, are mesenchymal stem cells still relevant? Frontiers in Bioengineering and Biotechnology 8
7. Shirkoohi FJ, Ghollasi M, Halabian R, Eftekhari E, Ghiasi M (2024) Oxaloacetate as new inducer for osteogenic differentiation of human adipose tissue-derived mesenchymal stem cells in vitro. Mol Biol Rep 51:451
8. Zhu Y, Liu T, Song K, Fan X, Ma X, Cui Z (2008) Adipose-derived stem cell: a better stem cell than BMSC. Cell biochemistry and function: Cellular biochemistry and its modulation by active agents or disease. 26:664–675
9. Murata D, Kunitomi Y, Harada K, Tokunaga S, Takao S, Nakayama K (2020) Osteochondral regeneration using scaffold-free constructs of adipose tissue-derived mesenchymal stem cells made by a bio three-dimensional printer with a needle-array in rabbits. Regenerative Therapy 15:77–89
10. Ahmed TA, Dare EV, Hincke M (2008) Fibrin: a versatile scaffold for tissue engineering applications. Tissue Eng Part B: Reviews 14:199–215
11. Jahanbani Y, Davaran S, Ghahremani-Nasab M, Aghebati-Maleki L, Yousefi M (2020) Scaffold-based tissue engineering approaches in treating infertility. Life Sci 240:117066
12. Chan BP, Leong KW (2008) Scaffolding in tissue engineering: general approaches and tissue-specific considerations. Eur Spine J 17(Suppl 4):467–479
13. Discher DE, Janmey P, Wang Y-l (2005) Tissue cells feel and respond to the stiffness of their substrate. Science 310:1139–1143
14. Ghassemi T, Shahroodi A, Ebrahimzadeh MH, Mousavian A, Movaffagh J, Moradi A (2018) Current concepts in scaffolding for bone tissue Engineering. Arch Bone Jt Surg 6:90–99
15. Balaji Raghavendran HR, Puvaneswary S, Talebian S et al (2014) A comparative study on in vitro osteogenic priming potential of electron spun scaffold PLLA/HA/Col, PLLA/HA, and PLLA/Col for tissue engineering application. PLoS ONE 9, e104389
16. Soraya Z, Ghollasi M, Halabian R, Eftekhari E, Tabasi A, Salimi A (2021) Donepezil hydrochloride as a novel inducer for osteogenic differentiation of mesenchymal stem cells on PLLA scaffolds in vitro. Biotechnol J, 2100112
17. Mei F, Zhong J, Yang X et al (2007) Improved biological characteristics of poly (L-lactic acid) electrospun membrane by incorporation of multiwalled carbon nanotubes/hydroxyapatite nanoparticles. Biomacromolecules 8:3729–3735
18. Liao L, Yang S, Miron RJ, Wei J, Zhang Y, Zhang M (2014) Osteogenic properties of PBLG-g-HA/PLLA nanocomposites. PLoS ONE 9, e105876
19. Ribas RG, Schatkoski VM, Montanheiro TLA et al (2019) Current advances in bone tissue engineering concerning ceramic and bioglass scaffolds: a review. Ceram Int 45:21051–21061
20. Pantulap U, Arango-Ospina M, Boccaccini AR (2022) Bioactive glasses incorporating less-common ions to improve biological and physical properties. J Mater Science: Mater Med 33:1–41
21. Saino E, Grandi S, Quartarone E et al (2011) In vitro calcified matrix deposition by human osteoblasts onto a zinc-containing bioactive glass. Eur Cell Mater 21:59–72
22. Riva F, Bloise N, Omes C et al (2023) Human ovarian follicular fluid mesenchymal stem cells Express osteogenic markers when cultured on Bioglass 58S-Coated Titanium scaffolds. Materials 16:3676
23. Mortazavi V, Nahrkhalaji MM, Fathi M, Mousavi S, Esfahani BN (2010) Antibacterial effects of sol-gel-derived bioactive glass nanoparticle on aerobic bacteria. Journal of Biomedical materials Research Part A: an Official Journal of the Society for Biomaterials, the Japanese Society for Biomaterials, and the Australian Society for Biomaterials and the Korean. Soc Biomaterials 94:160–168
24. Gong WY, Dong YM, Chen XF, Karabucak B (2012) Nano-sized 58S bioactive glass enhances proliferation and osteogenic genes expression of osteoblast-like cells. Chin J Dent Res 15:145
25. Haddadi MH, Karamian E, Bakhsheshi-Rad HR, Kasiri-Asgarani M (2023) Investigation of the effect of Bioglass-58S content on structural and biological properties of PCL-chitosan-58S-bioactive glass composite coating for bone tissue engineering application. Ceram Int 49:8190–8195
26. Joughehdoust S, Manafi S (2012) Synthesis and in vitro investigation of sol-gel derived bioglass-58S nanopowders. Mater Science-Poland 30:45–52
27. Kokubo T, Takadama H (2006) How useful is SBF in predicting in vivo bone bioactivity? Biomaterials 27:2907–2915
28. Niu Y, Guo L, Liu J et al (2015) Bioactive and degradable scaffolds of the mesoporous bioglass and poly (L-lactide) composite for bone tissue regeneration. J Mater Chem B 3:2962–2970
29. Conoscenti G, Carfi Pavia F, Ciraldo FE et al (2018) In vitro degradation and bioactivity of composite poly-l-lactic (PLLA)/bioactive glass (BG) scaffolds: comparison of 45S5 and 1393BG compositions. J Mater Sci 53:2362–2374
30. Nezafati N, Moztarzadeh F, Hesaraki S (2012) Surface reactivity and in vitro biological evaluation of sol gel derived silver/calcium silicophosphate bioactive glass. Biotechnol Bioprocess Eng 17:746–754
31. Rohani Z, Ghollasi M, Aghamollaei H et al (2022) A new hydrogel with fluorapatite nanoparticles for osteogenic differentiation of human adipose-derived stem cells in tissue engineering field. Cell Tissue Res, 1–13
32. Zhu D-Y, Lu B, Yin J-H et al (2019) Gadolinium-doped bioglass scaffolds promote osteogenic differentiation of hBMSC via the Akt/GSK3β pathway and facilitate bone repair in vivo. Int J Nanomed, 1085–1100
33. Schrooten J, Helsen J (2000) Adhesion of bioactive glass coating to Ti6Al4V oral implant. Biomaterials 21:1461–1469
34. Sepulveda P, Jones JR, Hench LL (2002) Bioactive sol-gel foams for tissue repair. J Biomedical Mater Research: Official J Soc Biomaterials Japanese Soc Biomaterials Australian Soc Biomaterials Korean Soc Biomaterials 59:340–348
35. Yang XB, Webb D, Blaker J et al (2006) Evaluation of human bone marrow stromal cell growth on biodegradable polymer/Bioglass® composites. Biochem Biophys Res Commun 342:1098–1107
36. Fathi M, Doostmohammadi A (2009) Bioactive glass nanopowder and bioglass coating for biocompatibility improvement of metallic implant. J Mater Process Technol 209:1385–1391
37. Li N, Jie Q, Zhu S, Wang R (2005) Preparation and characterization of macroporous sol–gel bioglass. Ceram Int 31:641–646
38. Moghanian A, Firoozi S, Tahriri M (2017) Synthesis and in vitro studies of sol-gel derived lithium substituted 58S bioactive glass. Ceram Int 43:12835–12843

39. Sepulveda P, Jones J, Hench L (2002) In vitro dissolution of melt-derived 45S5 and sol-gel derived 58S bioactive glasses. J Biomedical Mater Research: Official J Soc Biomaterials Japanese Soc Biomaterials Australian Soc Biomaterials Korean Soc Biomaterials 61:301–311
40. Perardi A, Cerrruti M, Morterra C (2005) Carbonate formation on sol-gel bioactive glass 58S and on Bioglass® 45S5; in Studies in Surface Science and Catalysis 461–469, Elsevier
41. Cañaveral S, Morales D, Vargas AF (2019) Synthesis and characterization of a 58S bioglass modified with manganese by a sol-gel route. Mater Lett 255:126575
42. Vadera N, Ashokan A, Gowd GS et al (2015) Manganese doped nano-bioactive glass for magnetic resonance imaging. Mater Lett 160:335–338
43. Wu X, Meng G, Wang S, Wu F, Huang W, Gu Z (2015) Zn and Sr incorporated 64S bioglasses: material characterization, in-vitro bioactivity and mesenchymal stem cell responses. Mater Sci Engineering: C 52:242–250
44. Jell G, Stevens MM (2006) Gene activation by bioactive glasses. J Mater Science: Mater Med 17:997–1002
45. Molavi AM, Sadeghi-Avalshahr A, Nokhasteh S, Naderi-Meshkin H (2020) Enhanced biological properties of collagen/chitosan-coated poly(ε-caprolactone) scaffold by surface modification with GHK-Cu peptide and 58S bioglass. Prog Biomater 9:25–34
46. Subbiah T, Bhat GS, Tock RW, Parameswaran S, Ramkumar SS (2005) Electrospinning of nanofibers. J Appl Polym Sci 96:557–569
47. Baino F (2018) Bioactive glasses–when glass science and technology meet regenerative medicine. Ceram Int 44:14953–14966
48. Hafezi M, Safarian S, Khorasani MT, Osman NAA (2016) Polyurethane/58S bioglass nanofibers: synthesis, characterization, and in vitro evaluation. RSC Adv 6:35815–35824
49. Radev L, Zheleva D, Michailova I (2013) In vitro bioactivity of Polyurethane/85S Bioglass composite scaffolds. Cent Eur J Chem 11:1439–1446
50. Shahrbabak MSN, Sharifianjazi F, Rahban D, Salimi A (2019) A comparative investigation on bioactivity and antibacterial properties of sol-gel derived 58S bioactive glass substituted by Ag and Zn. Silicon 11:2741–2751
51. Barrioni BR, Norris E, Li S, Naruphontjirakul P, Jones JR, Pereira MdM (2019) Osteogenic potential of sol–gel bioactive glasses containing manganese. J Mater Science: Mater Med 30:1–15
52. Hoppe A, Güldal NS, Boccaccini AR (2011) A review of the biological response to ionic dissolution products from bioactive glasses and glass-ceramics. Biomaterials 32:2757–2774
53. Yao Q, Liu H, Lin X et al (2019) 3D interpenetrated graphene foam/58S bioactive glass scaffolds for electrical-stimulation-assisted differentiation of rabbit mesenchymal stem cells to enhance bone regeneration. J Biomed Nanotechnol 15:602–611
54. El-Gendy R, Yang XB, Newby PJ, Boccaccini AR, Kirkham J (2013) Osteogenic differentiation of human dental pulp stromal cells on 45S5 Bioglass® based scaffolds in vitro and in vivo. Tissue Eng Part A 19:707–715
55. Lee JM, Kim MG, Byun JH et al (2017) The effect of biomechanical stimulation on osteoblast differentiation of human jaw periosteum-derived stem cells. Maxillofac Plast Reconstr Surg 39:7
56. Koblenzer M, Weiler M, Fragoulis A, Rütten S, Pufe T, Jahr H (2022) Physiological mineralization during in Vitro Osteogenesis in a Biomimetic Spheroid Culture Model. Cells 11
57. Meyer MB, Benkusky NA, Pike JW (2014) The RUNX2 cistrome in osteoblasts: Characterization, down-regulation following differentiation, and relationship to gene expression*. J Biol Chem 289:16016–16031
58. Termine JD, Kleinman HK, Whitson SW, Conn KM, McGarvey ML, Martin GR (1981) Osteonectin, a bone-specific protein linking mineral to collagen. Cell 26:99–105
59. Lin X, Patil S, Gao YG, Qian A (2020) The bone extracellular matrix in bone formation and regeneration. Front Pharmacol 11:757
60. Wang JS, Mazur CM, Wein MN (2021) Sclerostin and osteocalcin: candidate bone-produced hormones. Front Endocrinol (Lausanne) 12:584147
61. Leucht P, Lee S, Yim N (2019) Wnt signaling and bone regeneration: can't have one without the other. Biomaterials 196:46–50
62. Qu B, Liu BR, Du YJ et al (2014) Wnt/β–catenin signaling pathway may regulate the expression of angiogenic growth factors in hepatocellular carcinoma. Oncol Lett 7:1175–1178